ACS APPLIED MATERIALS & INTERFACES

Letter

www.acsami.org

Macroscopic Architecture of Charge Transfer-Induced Molecular Recognition from Electron-Rich Polymer Interpenetrated Porous Frameworks

Linyi Bai,[†] Peng Wang,[†] Purnandhu Bose,[†] Peizhou Li,[†] Ruqiang Zou,*[,‡,§] and Yanli Zhao*[,†,§,#]

[†]Division of Chemistry and Biological Chemistry, School of Physical and Mathematical Sciences, Nanyang Technological University, 21 Nanyang Link, Singapore 637371

[‡]Department of Materials Science and Engineering, College of Engineering, Peking University, Beijing 100871, PR China

[§]Singapore Peking University Research Centre for a Sustainable Low-Carbon Future, 1 Create Way, Singapore 138602

[#]School of Materials Science and Engineering, Nanyang Technological University, 50 Nanyang Avenue, Singapore 639798

Supporting Information

ABSTRACT: Fluorescent and electron-rich polymer threaded into porous framework provides a scaffold for sensing acceptor molecules through noncovalent interactions. Herein, poly(9-vinylcarbazole) (PVK) threaded MIL-101 with confined nanospace was synthesized by vinyl-monomer impregnation, in situ polymerization, and interpenetration. The pore size of the resulted hybrid could be controlled by varying the time of polymerization and interpenetration. The interaction of PVK-threaded MIL-101 with guest molecules showed a charge-transfer progress with an obvious red shift in the optical spectra. Depending on the degree of the interaction, the solution color changed from blue to green or to yellow. In particular, electron-rich PVK-threaded MIL-101 could effectively probe electron-poor nitro compounds, especially 1,3,5-trinitrobenzene (TNP), a highly explosive material. This sensing approach is a colorimetric methodology, which is very simple and convenient for practical analysis and operation.

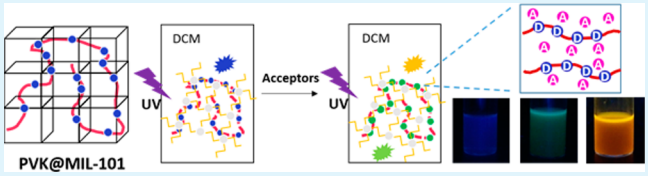

KEYWORDS: *charge transfer, interpenetration, metal−organic frameworks, molecular recognition, nitro explosive*

Porous coordinated polymers[1,2] and complex networks,[3,4] particularly metal−organic frameworks (MOFs)[5−7] and their variations, have been rapidly developed into a novel class of porous materials. In addition to the properties such as diverse functionalities, high surface areas, and high porosities, MOFs integrate the advantages of ceramic matrix and regular pore structures, capable of storing specific guest molecules.[8,9] Because the inclusion of appropriate guest molecules within MOFs is restricted by chemical affinity of the porous cavities, functionalizing the pore structures is an efficient approach to improve the host−guest interactions. The pioneering work has demonstrated that the introduction of extra functional species into MOFs can lead to increased adaptability for the encapsulation of guest molecules.[10−13] Recently, Gao and co-workers[14] reported that a monomer could be caged into ZIF-8, where it formed a macromolecule by polymerization. The caged hybrid showed superior performance of ion exchange.

However, utilizing MOFs' inherent advantages of high porosity and controlled swelling to cage functional polymers inside for molecular recognition with high selectivity controlled by different size of pores has not been well investigated. Comparing with conventional materials for molecular recognition, a synergy effect is expected in the present case, where polymer-threaded MOFs enhance the stability of the hybrids and the MOF porosity could be used to realize the selectivity toward different guest molecules. Some guest molecules with large sizes cannot enter into the polymer-caged MOFs, so that no interaction happens. On the other hand, those small guest molecules can go inside and move freely, interacting with the polymer inside MOFs.

In our present work, we envisioned that the flexible nanospace between MOF and polymer would show specific guest adsorption via the donor−acceptor interactions, which could be used for specific guest recognition. We made use of the advantages of MOFs with high porosity and controlled swelling to cage one electron-rich polymer into the MOF cavities, and the resultant hybrid material as a new detection system showed a special interaction with some electron-acceptor molecules, particularly nitro compounds, due to the electron donor−acceptor effect. Since nitro compounds are the major components in explosive, it is very important to detect and control their concentrations before any utilization.[15−17] In this case, the recognition of guest molecules can be detected by fluorescence. The fluorescence of polymer-threaded MOF is highly sensitive to the surrounding conditions, and thus the effect of incorporating various guests into the nanospace can be manifested either by the changes in the emission intensity or by

Received: December 26, 2014
Accepted: February 24, 2015
Published: February 24, 2015

DOI: 10.1021/am5089549
ACS Appl. Mater. Interfaces 2015, 7, 5056−5060

the appearance of a new emission band on account of exciplex/excimer formation or charge transfer (CT).[18,19]

The nitro compounds generally have low electron intensity with a pull-electron effect. Electron-rich materials are desired to probe the nitro compounds toward practical applications. Herein, we developed electron-rich polymer-caged MOF to detect the concentration of 1,3,5-trinitrobenzene (TNP), a highly explosive material, through obvious red shift on optical spectra and visible color change. Some studies about the TNP detection have been reported, including the utilizations of fluorescent quenching effect,[15,17,20,21] conjugated chromophores,[22,23] and metal coordination.[24−26] To the best of our knowledge, the present study is the first example for the detection of nitro compounds using polymer-caged MOF.

MIL-101 is a superstar in the MOF family, because of its excellent characteristics in terms of cell dimension, pore size and surface area, which was first synthesized by G. Férey and co-workers.[27] It possesses large spherical cavities with diameter of ∼2.9 nm, and the pore size of the windows is 1.2−1.6 nm. On account of the large pore size, it was chosen as a suitable porous material for caging functional molecules. Several studies have been reported in the past few years using caged and covered MIL-101 for catalysis, adsorption and morphology control.[28,29] In our present study, we initially predicted the loading of a monomer into the MIL-101 cavities through computational calculations (Figure S1 in the Supporting Information). 9-Vinylcarbazole has a molecular size of 7.1 × 8.2 Å^2, which is much smaller than the porosity of MIL-101. It means that this molecule is able to impregnate into the MIL-101 cavities completely. Supported by the calculations, we designed polymer-caged MIL-101. MIL-101 was first activated under vacuum in 150 °C for 6 h, so that the solvent molecules in the cavities could be removed. Then, 9-vinylcarbazole monomer and azobis(isobutyronitrile) initiator in dichloromethane (DCM) were added, the resulted mixture was stirred for overnight to ensure the encapsulation of the monomer into the cavities. After solvothermal reaction for the formation of poly(9-vinylcarbazole) (PVK) inside MIL-101, the remaining monomer, oligomer, and those species stayed on the surface of MIL-101 were washed away by acetone through the Soxhelt extraction. Finally, the obtained PVK caged MIL-101 (PVK@MIL-101) powder was dried for further uses (see Figure 1 and experimental section in the Supporting Information). After loading PVK into the cavities, MIL-101 showed strong blue fluorescence under UV lamp.

The synthesized PVK@MIL-101 was fully characterized by scanning electron microscope (SEM), powder X-ray diffraction (PXRD), N_2 adsorption/desorption measurements, and Fourier transform infrared spectroscopy (FTIR). As seen from the SEM images (Figure 2), PVK@MIL-101 is micrometer scale particles, and the surface of the particles after caging the polymer is still smooth as original ones. Moreover, no obvious enhancement of the particle diameter was observed after the polymer encapsulation.

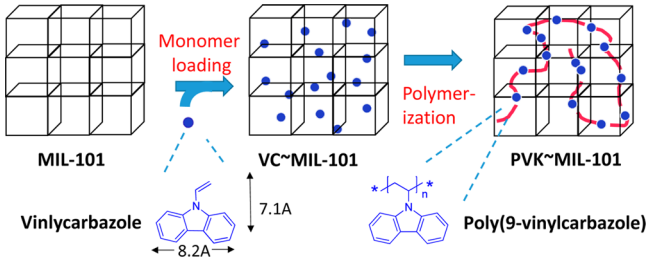

Figure 1. Schematic illustration for the synthesis of electron-rich PVK polymer-caged MOF (PVK@MIL-101) from monomer loading to the polymerization in the porous network of MIL-101.

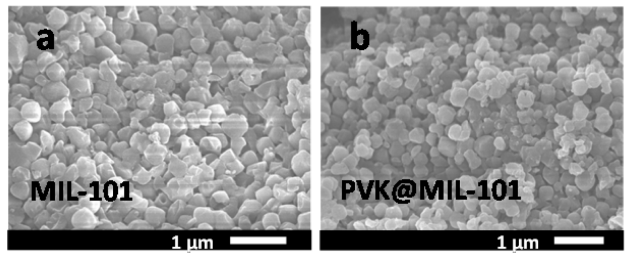

Figure 2. SEM images of MIL-101 (a) before and (b) after caging polymer.

From the PXRD patterns (Figure 3a), MIL-101 structure in the synthesized PVK@MIL-101 remained intact, and several key diffraction peaks match with that of original MIL-101. As compared with the PXRD pattern of original MIL-101, some slight shifts in the PXRD peaks were observed, corresponding to a very small expansion after the polymer caging. Physical mixing of MOFs and organic compounds showed no shifts in the PXRD patterns. The broad peak around 20° was assigned to the polymer threading in MIL-101. This conclusion was also supported by FTIR spectra with the appearance of quaternary peaks for the polymer at ca. 3051, 2946, 1453, and 715 cm^{-1}

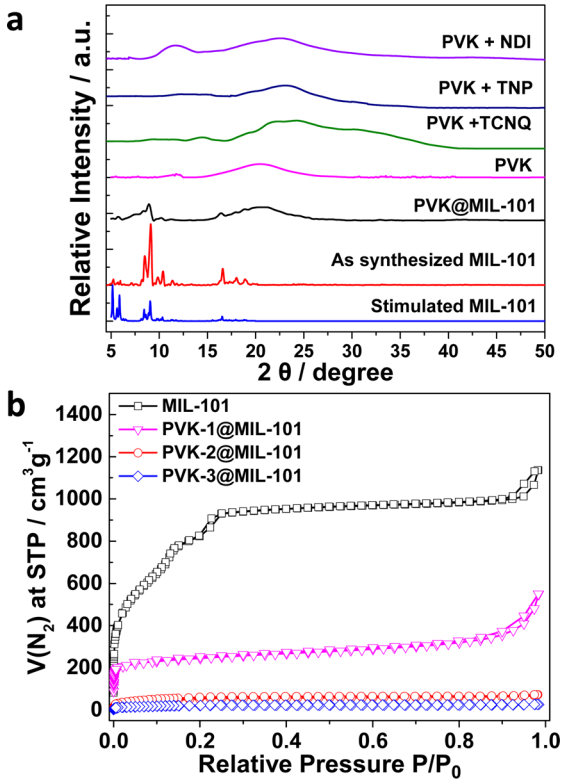

Figure 3. (a) PXRD patterns of MIL-101 before (blue curve) and after (red curve) caging polymer; (b) N_2 adsorption/desorption isotherms at 77K for MIL-101 before (black curve) and after caging different polymers obtained under different polymerization times. Purple, red, and blue curves indicate 1, 2, and 3 days of reactions, respectively.

DOI: 10.1021/am5089549
ACS Appl. Mater. Interfaces 2015, 7, 5056−5060

(Figure S2 in the Supporting Information). The reason that the polymer interpenetrates into the framework cavities and does not cover on the surface is discussed as follows. By interpenetrating into the cavities, the polymer has the ability to influence the pore size with different degree depending on the reaction time. Figure 3b shows N_2 adsorption/desorption isotherms at 77K for MIL-101 before and after caging the polymer under different polymerization times of 1 day, 2 days and 3 days. It could be clearly found that the polymers obtained under different polymerization time were able to influence the adsorption capability of MIL-101 at different degrees. In other words, it can tune the porous size of MIL-101 with the maximum surface area of 1134 $m^2 g^{-1}$ (Table 1). If the polymer just covers the surface of MIL-101, the adsorption value should be much lower than this value. To evaluate the polymerization degree of the monomer, we tested the number-averaged molecular weights (Mw) of the polymers by matrix-assisted laser desorption/ionization time-of-flight (MALDI TOF) mass spectrometry after removing the MIL-101 host through base washing (Figure S3 in the Supporting Information). The M_w values of the three polymers are 2032, 3128, and 5221, corresponding to ~10, ~16, and ~27 monomer units, respectively. On the basis of the controlled polymerization, it is possible to tune the pore size of MIL-101 by caging the polymer. On the other hand, the MIL-101 framework can also influence the polymer growth degree.

Table 1. Structural and Polymer-Caged Properties of MIL-101 and PVK@MIL-101

sample	S_{BET} (m^2/g)[a]	pore width (nm)[b]	degradation temperature (°C)[c]
MIL-101	~1709	2.4	~394
PVK-1@MIL-101 (1 day)	~1134	1.0	~379
PVK-2@MIL-101 (2 days)	~128	1.8	
PVK-3@MIL-101 (3 days)	~123	1.4	

[a]Determined by N_2 adsorption/desorption isotherms at 77K; [b]determined by Hohenberg−Kohn (HK) model of slit pore, which gives the correct value of 0.5 nm for a standard zeolite 5 Å. Alternative density functional theory (DFT) analysis based on cylindrical pore shape gives 2.4 nm for MIL-101 and 1.0 nm for PVK-1@MIL-101; [c]From TGA results in Figure S5 in the Supporting Information.

The pore width distribution of MIL-101 after caging the polymer provides further evidence for the porosity decrease (Figure S4 in the Supporting Information). The three polymers obtained with different polymerization times could reduce the pore sizes from original 2.4 to 1.0, 1.8, and 1.4 nm, respectively (Table 1), indicating that the pore size distribution does not change upon the impregnation process. Instead, the microporous region (<2 nm) is more strongly affected, because micropores contribute more to the pore volume and surface area, which could be observed from dramatic decrease of the pore volume in this region as compared to the reduction in mesopore region. The pore volume and area of micropores and mesopores are summarized in Table S1 (Supporting Information). For MIL-101 and PVK-1@MIL-101, the micropore volumes are 1.352 cc/g and 0.502 cc/g respectively, while the corresponding total pore volumes are 1.757 and 0.978 cc/g. In terms of the surface area, the major contribution is also provided by the micropores. The observations suggest that the caged polymer is not only at mesoporous region, but also surrounds the supertetrahedron to clog the micropores. In addition, the degradation temperature of PVK@MIL-101 obtained by thermogravimetric analysis (TGA) is another evidence to support the polymer interpenetration into the cavity, but not on the surface (Figure S5 in the Supporting Information). One obvious weight loss for MIL-101 without polymer was observed below 100 °C, on account of the solvent removal from the cavities. However, a same weight loss temperature cannot be found for the case of PVK@MIL-101. This observation indicates that the polymer was caged into the

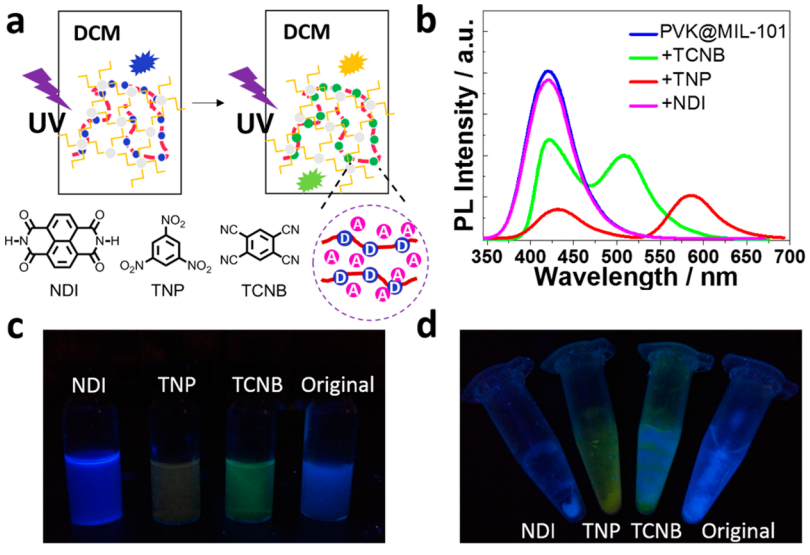

Figure 4. (a) Schematic representation of using PVK@MIL-101 to recognize three acceptors, i.e., NDI, TNP, and TCNB. The circle figure shows the CT process. (b) Fluorescence spectra of PVK@MIL-101 before (blue) and after introducing three acceptors (green for TCNB, red for TNP, and purple for NDI). (c) The emission of PVK@MIL-101 in solution under UV lamp before and after interacting with the three molecules. The right one is the original solution of PVK@MIL-101 without any acceptors. (d) The emission of PVK@MIL-101 in the solid state (obtained by centrifugation) under UV lamp before and after interacting with three acceptors. The right one is PVK@MIL-101 without any acceptors.

DOI: 10.1021/am5089549
ACS Appl. Mater. Interfaces 2015, 7, 5056−5060

framework, where the polymer replaced the solvent molecule and occupied the cavities.

As above-mentioned, the polymer caged into the MIL-101 cavities is an electron-rich component, and can interact with electron-deficient guest molecules through the CT process. Herein, PVK-1@MIL-101 prepared under 1 day polymerization was selected to recognize the acceptor molecules, due to its remained porosity. The remained pores could provide the selectivity to different acceptors with different sizes. The schematic illustration of the recognition process is shown in Figure 4a. We chose three traditional acceptor molecules with different molecular sizes (Figure S1 in the Supporting Information), i.e., 1,4,5,8-naphthalenetetracarboxdiimide (NDI), TNP, and tetracyanobenzene (TCNB). These compounds were added into the dispersed solution of PVK-1@MIL-101 in DCM, where the compounds could dissolve in DCM for interacting with PVK-1@MIL-101. The adsorption and emission spectra of PVK were previously investigated both in solution and film.[30] Under photoexcitation, PVK yields a broad fluorescence peak in the violet-blue region. Its high-energy emission centers at ~375 nm, whereas lower energy band is at ~420 nm in toluene. We also observed almost same fluorescence spectra for PVK in solution (Figure S6 in the Supporting Information).

The interaction of PVK@MIL-101 with these guests was probed by fluorescence (Figure 4b). In the fluorescence spectrum, a peak at longer wavelength represents the CT process. To further confirm the CT process, precise control experiments of the guests with polymer-caged MOF were carried out. The interaction of electron donor and acceptor was probed by the PXRD in situ (Figure 3a). The broad peak around 22° belongs to PVK before interacting with any acceptor. When an acceptor was introduced, a slight peak shift occurred, indicating the CT complex formation.[29] The process was also supported by cyclic voltammetry experiments (Figure S7 in the Supporting Information). It could be found that the oxidation potential decreased after interacting with electron deficient aromatics, meaning that the CT process occurred. In the fluorescent spectra, the interactions of TNP and TCNB with PVK@MIL-101 generated a peak at longer wavelength, while no obvious difference was observed in the case of NDI with PVK@MIL-101. The different phenomena were caused by the selectivity given by the remained pore of PVK@MIL-101. The sizes of these three acceptor molecules were predicted by theoretical calculation (Figure S1 in the Supporting Information). Although the size of NDI molecule is smaller than the pore, $\pi-\pi$ stacking aggregation among NDI molecule increases the volume, so that it cannot entry into the cavities to interact with the polymer inside. As the electron-withdrawing ability of TCNB is weaker than TNP, it is why the fluorescence red-shift degree of PVK@MIL-101 with TNP is bigger than that with TCNB. Moreover, the difference of emission color is very obvious under UV lamp (Figure 4c). The original color of PVK@MIL-101 dispersed in DCM is blue, originated from the caged polymer, while MIL-101 has no fluorescence. When the acceptor guests were added into the dispersion for several seconds, the color of the mixture changed obviously to green and yellow for TCNB and TNP, respectively. After centrifugation, the obtained solid powder was collected. It can be seen that the fluorescence color of PVK@MIL-101 powder before and after interacting with NDI still had no change (Figure 4d). The observation also supports the polymer interpenetration and the interaction with the acceptor guests inside the cavities, but not on the surface of MIL-101.

On the basis of the selectivity of PVK@MIL-101 toward different acceptors, we then utilized it as a detector for nitro compounds, especially for TNP, a highly explosive substance. In the optical spectra, one new peak was generated after treating PVK@MIL-101 with TNP, and the peak intensity became higher and higher upon increasing the interaction time (Figure S8 in the Supporting Information). The detection process is very quick within a few seconds. Particularly in the fluorescence spectra, the intensity of the original fluorescence peak around 425 nm for PVK@MIL-101 decreased after gradual addition of TNP, and the intensity of the newly generated peak around 582 nm increased upon time, matching well with the emission color change from blue to yellow. The fluorescence quenching at 425 nm is due to the interaction of caged polymer with electron-deficient TNP. The new peak at 582 nm was assigned to the CT process between the caged polymer and TNP. Upon increasing the time, the CT process became stronger, so that the peak intensity increased higher. The detection response is very sensitive and fast (less than 10 s) with a detection limit of up to 1 ppm (Figure S9 in the Supporting Information). In addition, we also tried to detect acceptors in vapor in order to indicate that this methodology could be applied in more common conditions. Here, the powder of PVK@MIL-101 was fixed on a glass substrate, which was then located on top of a container containing acetone at boiling point under heating (Figure S10 in the Supporting Information). It was observed that the fluorescence of PVK@MIL-101 was quenched upon time with a slightly bathochromic shift, supporting the interaction between PVK@MIL-101 and acetone.

In conclusion, we have reported a facile methodology to develop electron-rich polymer threaded MIL-101, featuring flexible nanospace for molecular recognition, particularly in the detection of TNP. The detection of nitro explosives using the polymer-caged MIL-101 through the CT process has been studied for the first time. The remained pores of MIL-101 after the polymer interpenetration provide the selectivity to various acceptor molecules with different sizes. The recognition of polymer-caged MIL-101 to certain guest molecules shows a characteristic red shift of the CT emission band, leading to a tunable emission profile. Superior detection performance of the polymer-caged MIL-101 toward TNP has been demonstrated. This approach of sensing TNP concentration by polymer-caged MOFs could be extended to other nitro compounds with suitable molecular size and electron donor−acceptor effect. The easy accessibility coupled with high surface area of the polymer-caged MIL-101 could enable the system to detect nitro explosives in gas phase or common environment, in which some conventional detecting systems showed poor performance owing to uncontrolled selectivity and inaccessibility of their embedded active sites. Therefore, the present work provides a simple and efficient approach for the fabrication of novel porous luminescent platforms in molecular recognition and detection.

■ ASSOCIATED CONTENT

Ⓢ Supporting Information

Additional theoretical calculations, polymer characterization, thermogravimetric analysis, cyclic voltammogram curves, and optical spectra. This material is available free of charge via the Internet at http://pubs.acs.org.

DOI: 10.1021/am5089549
ACS Appl. Mater. Interfaces 2015, 7, 5056−5060

AUTHOR INFORMATION

Corresponding Authors

*E-mail: zhaoyanli@ntu.edu.sg.
*E-mail: rzou@pku.edu.cn.

Notes

The authors declare no competing financial interest.

ACKNOWLEDGMENTS

This work is supported by the National Research Foundation (NRF), Prime Minister's Office, Singapore under its NRF Fellowship (NRF2009NRF-RF001-015) and Campus for Research Excellence and Technological Enterprise (CREATE) Programme—Singapore Peking University Research Centre for a Sustainable Low-Carbon Future, as well as the NTU-A*Star Centre of Excellence for Silicon Technologies (A*Star SERC 112 351 0003).

REFERENCES

(1) Uemura, T.; Yanai, N.; Kitagawa, S. Polymerization Reactions in Porous Coordination Polymers. *Chem. Soc. Rev.* **2009**, *38*, 1228−1236.

(2) Reboul, J.; Furukawa, S.; Horike, N.; Tsotsalas, M.; Hirai, K.; Uehara, H.; Kondo, M.; Louvain, N.; Sakata, O.; Kitagawa, S. Mesoscopic Architectures of Porous Coordination Polymers Fabricated by Pseudomorphic Replication. *Nat. Mater.* **2012**, *11*, 717−723.

(3) de Haan, L. T.; Sanchez-Somolinos, C.; Bastiaansen, C. M. W.; Schenning, A. P. H. J.; Broer, D. J. Engineering of Complex Order and the Macroscopic Deformation of Liquid Crystal Polymer Networks. *Angew. Chem., Int. Ed.* **2012**, *51*, 12469−12472.

(4) Fukino, T.; Joo, H.; Hisada, Y.; Obana, M.; Yamagishi, H.; Hikima, T.; Takata, M.; Fujita, N.; Aida, T. Manipulation of Discrete Nanostructures by Selective Modulation of Noncovalent Forces. *Science* **2014**, *344*, 499−504.

(5) Wang, C.; Liu, D.; Lin, W. Metal-Organic Frameworks as A Tunable Platform for Designing Functional Molecular Materials. *J. Am. Chem. Soc.* **2013**, *135*, 13222−13234.

(6) Li, J.-R.; Yu, J.; Lu, W.; Sun, L.-B.; Sculley, J.; Balbuena, P. B.; Zhou, H.-C. Porous Materials with Pre-Designed Single-Molecule Traps for CO_2 Selective Adsorption. *Nat. Commun.* **2013**, *4*, 1538−1545.

(7) Sun, C.-Y.; Wang, X.-L.; Zhang, X.; Qin, C.; Li, P.; Su, Z.-M.; Zhu, D.-X.; Shan, G.-G.; Shao, K.-Z.; Wu, H.; Li, J. Efficient and Tunable White-Light Emission of Metal-Organic Frameworks by Iridium-Complex Encapsulation. *Nat. Commun.* **2013**, *4*, 2717−2724.

(8) Bennett, T. D.; Cheetham, A. K. Amorphous Metal-Organic Frameworks. *Acc. Chem. Res.* **2014**, *47*, 1555−1562.

(9) Zhou, H.-C.; Long, J. R.; Yaghi, O. M. Introduction to Metal-Organic Frameworks. *Chem. Rev.* **2012**, *112*, 673−674.

(10) Comotti, A.; Bracco, S.; Mauri, M.; Mottadelli, S.; Ben, T.; Qiu, S.; Sozzani, P. Confined Polymerization in Porous Organic Frameworks with an Ultrahigh Surface Area. *Angew. Chem., Int. Ed.* **2012**, *51*, 10136−10140.

(11) Yanai, N.; Uemura, T.; Kitagawa, S. Behavior of Binary Guests in a Porous Coordination Polymer. *Chem. Mater.* **2012**, *24*, 4744−4749.

(12) Uemura, T.; Ono, Y.; Hijikata, Y.; Kitagawa, S. Functionalization of Coordination Nanochannels for Controlling Tacticity in Radical Vinyl Polymerization. *J. Am. Chem. Soc.* **2010**, *132*, 4917−4924.

(13) Distefano, G.; Suzuki, H.; Tsujimoto, M.; Isoda, S.; Bracco, S.; Comotti, A.; Sozzani, P.; Uemura, T.; Kitagawa, S. Highly Ordered Alignment of a Vinyl Polymer by Host-Guest Cross-Polymerization. *Nat. Chem.* **2013**, *5*, 335−341.

(14) Gao, L.; Li, C.-Y. V.; Chan, K.-Y.; Chen, Z.-N. Metal-Organic Framework Threaded with Aminated Polymer Formed in Situ for Fast and Reversible Ion Exchange. *J. Am. Chem. Soc.* **2014**, *136*, 7209−7212.

(15) Thomas, S. W., III; Joly, G. D.; Swager, T. M. Chemical Sensors Based on Amplifying Fluorescent Conjugated Oolymers. *Chem. Rev.* **2007**, *107*, 1339−1386.

(16) Hu, Z.; Deibert, B. J.; Li, J. Luminescent Metal-Organic Frameworks for Chemical Sensing and Explosive Detection. *Chem. Soc. Rev.* **2014**, *43*, 5815−5840.

(17) Salinas, Y.; Martinez-Manez, R.; Marcos, M. D.; Sancenon, F.; Costero, A. M.; Parra, M.; Gil, S. Optical Chemosensors and Reagents to Detect Explosives. *Chem. Soc. Rev.* **2012**, *41*, 1261−1296.

(18) Lei, Y. L.; Jin, Y.; Zhou, D. Y.; Gu, W.; Shi, X. B.; Liao, L. S.; Lee, S. T. White-Light Emitting Microtubes of Mixed Organic Charge-Transfer Complexes. *Adv. Mater.* **2012**, *24*, 5345−5351.

(19) Park, S. K.; Varghese, S.; Kim, J. H.; Yoon, S. J.; Kwon, O. K.; An, B. K.; Gierschner, J.; Park, S. Y. Tailor-Made Highly Luminescent and Ambipolar Transporting Organic Mixed Stacked Charge-Transfer Crystals: An Isometric Donor-Acceptor Approach. *J. Am. Chem. Soc.* **2013**, *135*, 4757−4764.

(20) Lan, A.; Li, K.; Wu, H.; Olson, D. H.; Emge, T. J.; Ki, W.; Hong, M.; Li, J. A Luminescent Microporous Metal-Organic Framework for the Fast and Reversible Detection of High Explosives. *Angew. Chem., Int. Ed.* **2009**, *48*, 2334−2338.

(21) Pramanik, S.; Zheng, C.; Zhang, X.; Emge, T. J.; Li, J. New Microporous Metal-Organic Framework Demonstrating Unique Selectivity for Detection of High Explosives and Aromatic Compounds. *J. Am. Chem. Soc.* **2011**, *133*, 4153−4155.

(22) Duncan, T. V.; Ishizuka, T.; Therien, M. J. Molecular Engineering of Intensely Near-Infrared Absorbing Excited States in Highly Conjugated Oligo(porphinato)zinc-(Polypyridyl)metal(II) Supermolecules. *J. Am. Chem. Soc.* **2007**, *129*, 9691−9703.

(23) Uyeda, H. T.; Zhao, Y. X.; Wostyn, K.; Asselberghs, I.; Clays, K.; Persoons, A.; Therien, M. J. Unusual Frequency Dispersion Effects of the Nonlinear Optical Response in Highly Conjugated (Polypyridyl)-metal-(Porphinato)zinc(II) Chromophores. *J. Am. Chem. Soc.* **2002**, *124*, 13806−13813.

(24) Gong, Y.-N.; Jiang, L.; Lu, T.-B. A Highly Stable Dynamic Fluorescent Metal-Organic Framework for Selective Sensing of Nitroaromatic Explosives. *Chem. Commun.* **2013**, *49*, 11113−11115.

(25) Xu, H.; Liu, F.; Cui, Y.; Chen, B.; Qian, G. A Luminescent Nanoscale Metal-Organic Framework for Sensing of Nitroaromatic Explosives. *Chem. Commun.* **2011**, *47*, 3153−3155.

(26) Zhang, S.-R.; Du, D.-Y.; Qin, J.-S.; Bao, S.-J.; Li, S.-L.; He, W.-W.; Lan, Y.-Q.; Shen, P.; Su, Z.-M. A Fluorescent Sensor for Highly Selective Detection of Nitroaromatic Explosives Based on a 2D, Extremely Stable, MetalOrganic Framework. *Chem.—Eur. J.* **2014**, *20*, 3589−3594.

(27) Ferey, G.; Mellot-Draznieks, C.; Serre, C.; Millange, F.; Dutour, J.; Surble, S.; Margiolaki, I. A Chromium Terephthalate-Based Solid with Unusually Large Pore Volumes and Surface Area. *Science* **2005**, *309*, 2040−2042.

(28) Aijaz, A.; Fujiwara, N.; Xu, Q. From Metal-Organic Framework to Nitrogen-Decorated Nanoporous Carbons: High CO_2 Uptake and Efficient Catalytic Oxygen Reduction. *J. Am. Chem. Soc.* **2014**, *136*, 6790−6793.

(29) Lu, G.; Li, S.; Guo, Z.; Farha, O. K.; Hauser, B. G.; Qi, X.; Wang, Y.; Wang, X.; Han, S.; Liu, X.; DuChene, J. S.; Zhang, H.; Zhang, Q.; Chen, X.; Ma, J.; Loo, S. C. J.; Wei, W. D.; Yang, Y.; Hupp, J. T.; Huo, F. Imparting Functionality to a Metal-Organic Framework Material by Controlled Nanoparticle Encapsulation. *Nat. Chem.* **2012**, *4*, 310−316.

(30) Klopffer, W. Transfer of Electronic Excitation Energy in Polyvinyl Carbazole. *J. Chem. Phys.* **1969**, *50*, 2337−2344.

DOI: 10.1021/am5089549
ACS Appl. Mater. Interfaces 2015, 7, 5056−5060